System Modeling and Design of a Hybrid Renewable Energy System for a Cable Network Head-End Station in Rural Area

Tobias Schillinger, Thomas Schuhmann and Martin Eckart
University of Applied Sciences Dresden
Friedrich-List-Platz 1
01069 Dresden, Germany
Phone: +49 (0) 351-4623068
Email: tobias.schillinger@htw-dresden.de
URL: https://www.htw-dresden.de/ema

Acknowledgements

This project is co-financed with tax funds on the basis of the budget passed by the Saxon State parliament.

Keywords

≪Renewable energy systems≫, ≪Simulation≫, ≪Energy system management≫, ≪Wind energy≫, ≪PV active generator≫

Abstract

This paper focuses on system modeling of a small scale renewable hybrid energy system for a cable network head-end station in rural areas located in central European lower mountain and lowland regions. Based on one year measured energy demand and local weather data the entire system model allows a location dependent energetic simulation and optimization for individual configurations of the photovoltaic, wind energy and battery storage systems. Using selected examples, different system configurations at varying locations are simulated and compared to each other with regard to the number of photovoltaic modules, size of the battery and power of the small wind turbine.

Introduction

The expansion of digital infrastructure in rural areas is accompanied by increasing energy demand of the signal processing systems and requires a high availability of the grid connection. The consequence of the loosely interconnected grid in rural areas is a high vulnerability with respect to power failures. Furthermore this development stands in contrast with the aim of reducing the reliance on fossile fuels. For these reasons it is necessary to crossover to decentralized sustainable energy systems with a high degree of self sufficiency, consisting of small wind energy, photovoltaic and battery storage systems. A further aspect is the relating reduction of the energy procurement costs. For this system the usage of second life lithium-ion traction batteries with a minimum residual capacity of approx. 80 % comes into question [1]. This paper describes a two stage energetic simulation of a hybrid renewable grid-connected energy system with a solar energy conversion system (SECS), small wind energy conversion system (WECS) and a battery energy storage system (BESS) in MATLAB/SIMULINK using the example of a cable network head-end station. Typically such stations convert incoming fiber optic signals and provide local broadband networks for small towns [2]. The structure of the proposed system is depicted in Fig. 1. The three subsystems, SECS, WECS & BESS, are modeled separately. Considering the losses of the power converters, every system is simulated with the MATLAB Parallel Computing Toolbox to obtain a subsystem model with reduced complexity based on characteristic diagrams. These lookup table (LUT) based subsystems are connected with an energy management system (EMS) to an entire system model which is

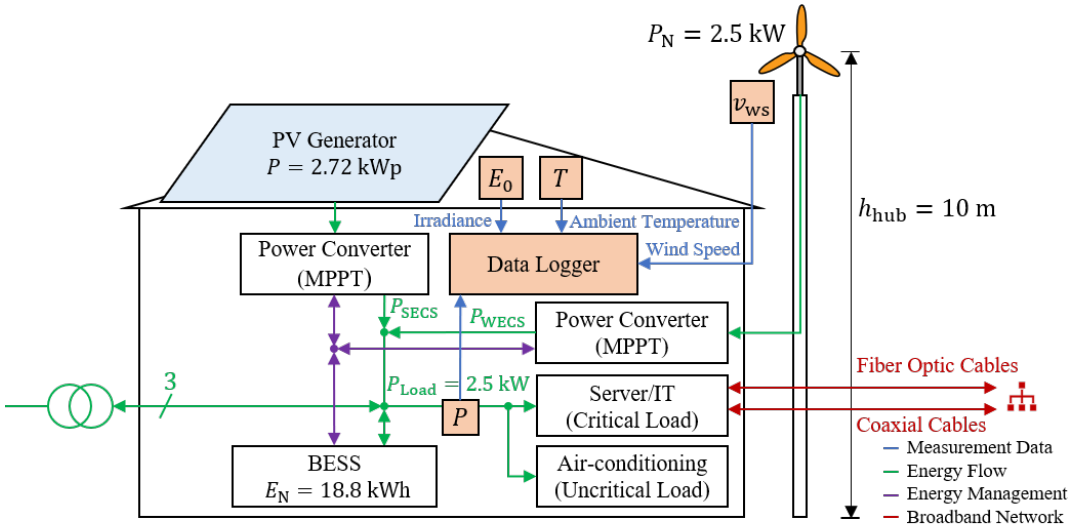

Fig. 1: Structure of the grid connected cable network head-end station with renewable energy and measurement system.

used for processig the measured annual data. These data were logged over a full year and include the energy demand of the three phase load, solar irradiance, ambient temperature and the wind speed. The load is divided into critical and not critical loads towards grid power failures.
This paper is organized as follows: The modeling aspects of the detailed subsystems and the entire system are given in the first section. The subsequent section presents the results of the simulation study based on four different exemplary locations as shown in Table V. In the conclusion, based on the simulation study, criteria for an optimal design of hybrid small-scale regenerative energy systems are discussed.

Modeling

System overview

The technical structure of the entire system model is shown in Fig. 2. The model is divided in three separate SIMULINK-models, SECS, WECS and BESS. A maximum power point tracking algorithm (MPPT) evaluates voltage and current from the PV array respectively the uncontrolled rectifier (B6U) of the wind generator system and controls the boost converter in the SECS and WECS. The two-level inverters are controlled by an inner current control and an outer DC voltage control loop. A phase locked loop calculates the phase angle for the Park transformation. The buck-boost converter controls the power flow for charging or discharing the battery. All power electronic components are modeled with Simscape insulated-gate-bipolar-transistors (IGBT). The operation point dependent losses of each IGBT are calculated based on [3] in combination with a thermal network of the heat sink. Typical IGBT characteristics are chosen from *Semikron skm50gb123D*.

Detailed modeling of system components

Two level inverter control

The single phase equivalent circuit of the three phase grid connected to the voltage source converter (VSC) is shown in Fig. 3. $\underline{v}_{VSC}$ is the voltage of the VSC, R_f the equivalent grid resistance, L_f the inductance, $\underline{v}_f$ and $\underline{i}_f$ are the grid voltage respectively current with the anguluar frequency ω_f. The following equation (1) describes the space vector model of this grid transformed to a coordinate system rotating with ω_f, the dq-system.

$$\vec{v}_{VSC}^{dq} = v_{VSC,d} + \mathrm{j}v_{VSC,q} = R_f \vec{i}_f^{dq} + L_f \frac{\mathrm{d}\vec{i}_f^{dq}}{\mathrm{d}t} + \mathrm{j}\omega_f L_f \vec{i}_f^{dq} + \vec{v}_f^{dq} \tag{1}$$

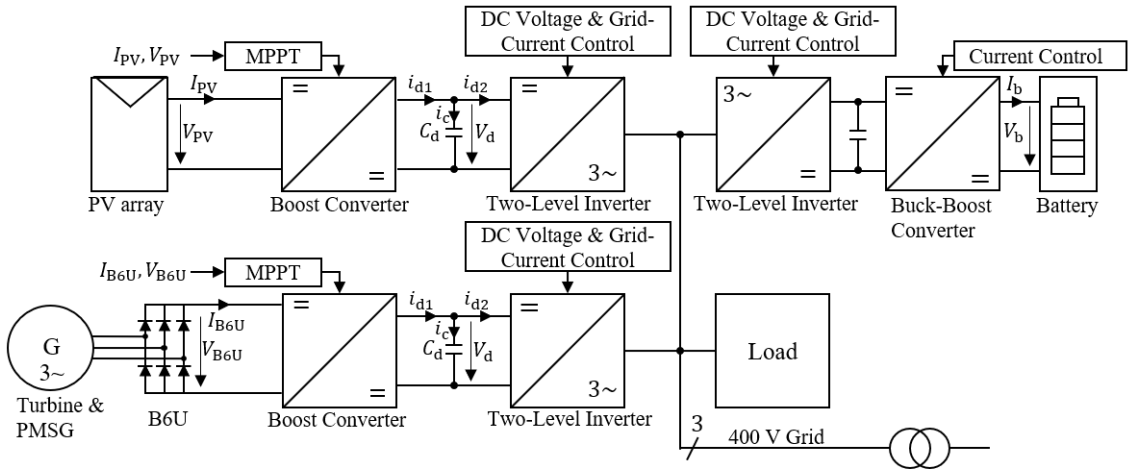

Fig. 2: Overview of the grid connected renewable energy system model.

After splitting up the $\mathcal{L}$-transfrom of (1) to its components and adding the following equations (2) for feed forward control, the transfer functions of the current control system are resulting to (3).

$$v_{\mathrm{ff,d}}(s) = -\omega_\mathrm{f} L_\mathrm{f} i_{\mathrm{f,q}}(s) + v_{\mathrm{f,d}}(s) \qquad v_{\mathrm{ff,q}}(s) = \omega_\mathrm{f} L_\mathrm{f} i_{\mathrm{f,d}}(s) + v_{\mathrm{f,q}}(s) \tag{2}$$

$$G_{\mathrm{f,d}}(s) = \frac{i_{\mathrm{f,d}}(s)}{v_{\mathrm{VSC,d}}(s)} = \frac{1/R_\mathrm{f}}{1 + s\frac{L_\mathrm{f}}{R_\mathrm{f}}} \qquad G_{\mathrm{f,q}}(s) = \frac{i_{\mathrm{f,q}}(s)}{v_{\mathrm{VSC,q}}(s)} = \frac{1/R_\mathrm{f}}{1 + s\frac{L_\mathrm{f}}{R_\mathrm{f}}} \tag{3}$$

The PI current controllers are adjusted with the Magnitude Optimum. The transfer function $G_{\mathrm{PI,i}}$, integral time $T_{\mathrm{I,i}}$, proportional gain $K_{\mathrm{P,i}}$ and the equivalent time constant T_eq considering the pulse frequency f_p are given in (4).

$$G_{\mathrm{PI,i}}(s) = K_{\mathrm{P,i}} \frac{1 + sT_{\mathrm{I,i}}}{sT_{\mathrm{I,i}}} \qquad T_{\mathrm{I,i}} = \frac{L_\mathrm{f}}{R_\mathrm{f}} \qquad K_{\mathrm{P,i}} = \frac{L_\mathrm{f}}{2\,T_{\mathrm{eq,i}}} \qquad T_{\mathrm{eq,i}} = \frac{1}{2\,f_\mathrm{p}} \tag{4}$$

For active power control the set point $i_{\mathrm{f,d,ref}}$ is calculated with (5) while $i_{\mathrm{f,q,ref}} = 0$.

$$P_\mathrm{f} = \frac{3}{2}\mathrm{Re}\left\{\vec{v}_\mathrm{f}^{\,\mathrm{dq}}\,\vec{i}_\mathrm{f}^{\,\mathrm{dq}*}\right\} = \frac{3}{2} v_{\mathrm{f,d}}\, i_{\mathrm{f,d}} \tag{5}$$

The current i_{d1} that comes from the preconnected system, e. g. PV array or uncontrolled rectifier, partially loads the DC link capacitance C_d, see (6). It results the input current i_{d2} of the VSC. Excluding the losses of the VSC, with the power balance (7) the integral time $T_{\mathrm{I,v}}$ and proportional gain $K_{\mathrm{P,v}}$ of the DC voltage PI controller $G_{\mathrm{PI,v}}$ (8) are calculated with the Symmetrical Optimum, as described in [4].

$$i_\mathrm{c} = i_{\mathrm{d1}} - i_{\mathrm{d2}} = C_\mathrm{d} \frac{\mathrm{d}v_\mathrm{d}}{\mathrm{d}t} \tag{6}$$

$$P_\mathrm{d} = P_\mathrm{f} = i_{\mathrm{d2}}\, v_\mathrm{d} \tag{7}$$

$$G_{\mathrm{PI,v}}(s) = K_{\mathrm{P,v}} \frac{1 + sT_{\mathrm{I,v}}}{sT_{\mathrm{I,v}}} \qquad T_{\mathrm{I,v}} = 32\,T_{\mathrm{eq,i}} \qquad K_{\mathrm{P,v}} = \frac{C_\mathrm{d}}{32\,T_{\mathrm{eq,i}}\,\frac{3}{2}\,\frac{v_{\mathrm{f,d}}}{V_{\mathrm{d,ref}}}} \tag{8}$$

Furthermore the switching signals for the IGBTs are generated with space vector modulation. The controlled two level inverter as a part of every subsystem is parametrized as follows:

$$R_\mathrm{f} = 1\,\Omega \quad L_\mathrm{f} = 1\,\mathrm{mH} \quad \omega_\mathrm{f} = 2\pi\,50\,\mathrm{s}^{-1} \quad \hat{v}_\mathrm{f} = 400\sqrt{2/3}\,\mathrm{V} \quad f_\mathrm{p} = 10\,\mathrm{kHz} \quad C_\mathrm{d} = 10\,\mathrm{mF}$$
$$V_{\mathrm{d,ref}} = 800\,\mathrm{V} \quad T_{\mathrm{I,i}} = 1\,\mathrm{ms} \qquad K_{\mathrm{P,i}} = 10\,\mathrm{V/A} \qquad T_{\mathrm{I,v}} = 1.6\,\mathrm{ms} \quad K_{\mathrm{P,v}} = 10.26\,\mathrm{A/V}$$

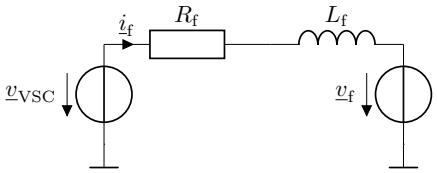

Fig. 3: Single phase equivalent circuit model of three phase grid with voltage source converter (VSC).

Solar energy conversion system

The Simscape photovoltaic (PV) array model is based on the dual resistance equivalent circuit [5], parametrized with data for the module Yingli YL170 (23)P, given in Table Ia. For MPPT a perturb-and-observe algorithm (P&O) is used, as described in [6]. The boost converter [7] inductance can be calculated by (10), the duty cycle with (9). Using the example of eight PV modules connected in series the resulting parameters are listed in Table Ib.

$$D_{\mathrm{V_{MPP}}} = 1 - \frac{V_\mathrm{MPP}}{V_\mathrm{d,ref}} \tag{9}$$

$$L = \frac{V_\mathrm{MPP}\, D_{\mathrm{V_{MPP}}}}{\Delta i_\mathrm{L}\, f_\mathrm{p}} \tag{10}$$

Table I: Parameterization of Simscape PV array with module data & boost converter.

(a) Parameterization of Simscape PV module.

Maximum Power	$P_\mathrm{max}\,/\,\mathrm{W}$	170
Cells per module	N_cell	48
Open circuit volage	$V_\mathrm{ocv}\,/\,\mathrm{V}$	29
Short circuit current	$I_\mathrm{sc}\,/\,\mathrm{A}$	8.1
Voltage at MPP	$V_\mathrm{MPP}\,/\,\mathrm{V}$	23
Current at MPP	$I_\mathrm{MPP}\,/\,\mathrm{A}$	7.39

(b) Parameterization of boost converter.

Switching frequncy	$f_\mathrm{p}\,/\,\mathrm{kHz}$	10
Modules in series	n_PV	8
Voltage at MPP	$V_\mathrm{MPP}\,/\,\mathrm{V}$	184
Duty cycle	$D_{\mathrm{V_{MPP}}}$	0.717
Current ripple	$\Delta i_\mathrm{L}\,/\,\mathrm{A}$	$0.2\, I_\mathrm{MPP}$
Inductance	$L\,/\,\mathrm{mH}$	8.93

Wind energy conversion system

The system model of the WECS is simulated as described in [8]. The P&O-algorithm varies the duty cycle of the boost converter. Using the Simscape permanent magnet synchronous generator (PMSG) model, the simulation is carried out using the configuration given in Table IV.

Table II: Parameter PMSG and Turbine for three different power ratings.

Nominal power	$P_\mathrm{N}\,/\,\mathrm{kW}$	2.5	5	7.5
Stator resistance	$R_\mathrm{s}\,/\,\Omega$	7.017	1.93	1.4
d-axis inductance	$L_\mathrm{d}\,/\,\mathrm{mH}$	41.27	13.41	7.82
q-axis inductance	$L_\mathrm{q}\,/\,\mathrm{mH}$	125	50	7.82
Permanent magnet flux linkage	$\Psi_\mathrm{PM}\,/\,\mathrm{Vs}$	0.79	2.45	3.18
Number of pole pairs	p	5	5	6
Turbine radius	$r\,/\,\mathrm{m}$	1.5	2.2	2.65

Battery energy storage system

A simplified single resistance model with a variable open circuit voltage (OCV) $V_{\mathrm{b},0}$ is used, shown in Fig. 4. As an example the battery capacity $Q_{\mathrm{b,N}}$ is chosen from the built in lithium-ion traction battery of the BMWi3, see [9]. Experimental measurements on this battery have shown an inner resistance about $R_\mathrm{b} = 0.1\,\Omega$. The Joule losses $P_{\mathrm{b,loss}}$ over R_b are calculated with (11). The state of charge (SOC) (12) results from the integration of the battery current I_b.

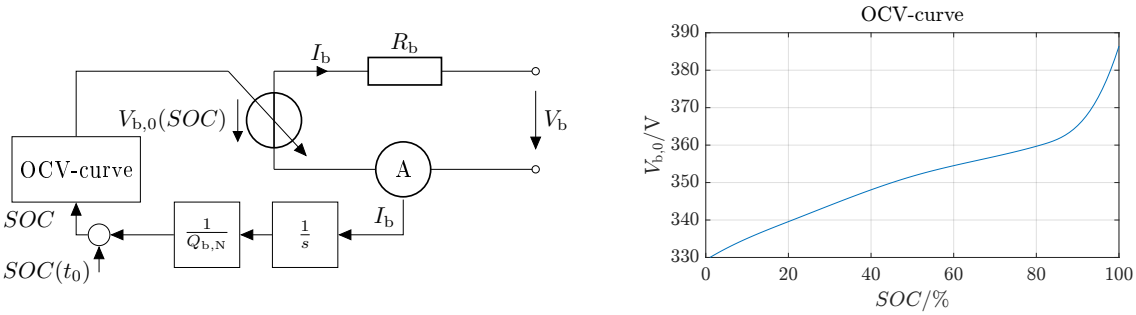

Fig. 4: Single resistance equivalent circuit & simulated OCV-curve of chosen lithium-ion battery.

$$P_{b,loss} = I_b^2 R_b \tag{11}$$

$$SOC(t) = SOC(t_0) + \frac{1}{Q_{b,N}} \int I_b \, dt \qquad \text{with} \qquad SOC_{min} \leq SOC \leq SOC_{max} \tag{12}$$

$$SOC_{min} = 0.05 \qquad SOC_{max} = 0.95$$

Two stage approach for system modeling

The two stage model approach is used to reduce the simulation effort. For this the detailed models of the SECS, WECS and BESS are simulated with predefined test vectors, see Table III, using the MATLAB Parallel Computing Toolbox. The fixed step size for simulation is 1 µs.

Table III: Test vectors for detailed loss modeling of SECS, WECS and BESS.

	SECS E_0 / (W/m²)	SECS T / °C	WECS v_w / (m/s)	BESS $P_{BESS,ref}$ / W
Minimum	100	-20	1	-10000
Increment	100	5	1	1000
Maximum	1400	40	15	10000

Using the example of the SECS, Fig. 5 shows the power flow of the system, considering the thermal losses from the switching components and cable connections. For this system all input combinations of E_0 and T are simulated until the steady state end values from thermal losses are reached. The simulation output is the resulting active power that is fed into the grid. Every output value is assigned to its input vector configuration and is saved to a LUT, shown in Fig. 6. The overall efficiency η for the SECS is calulated with the output power of the PV modules and the measured power after the VSC.

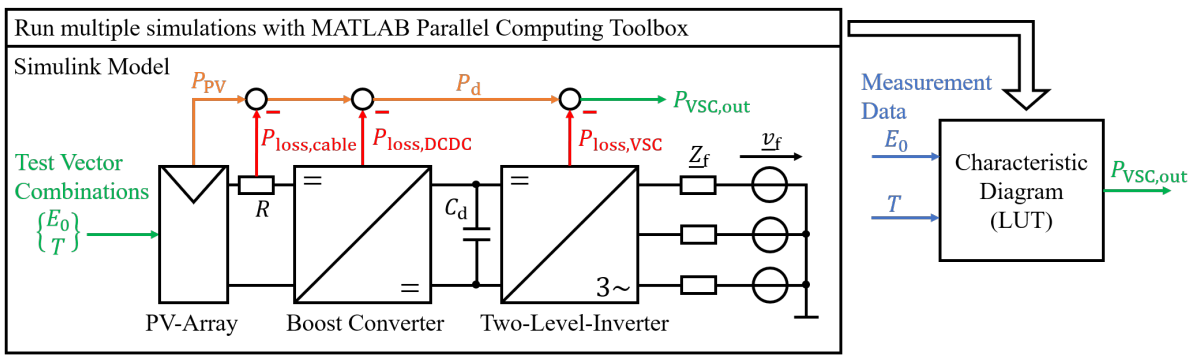

Fig. 5: Two model approach using the example of the solar energy conversion system.

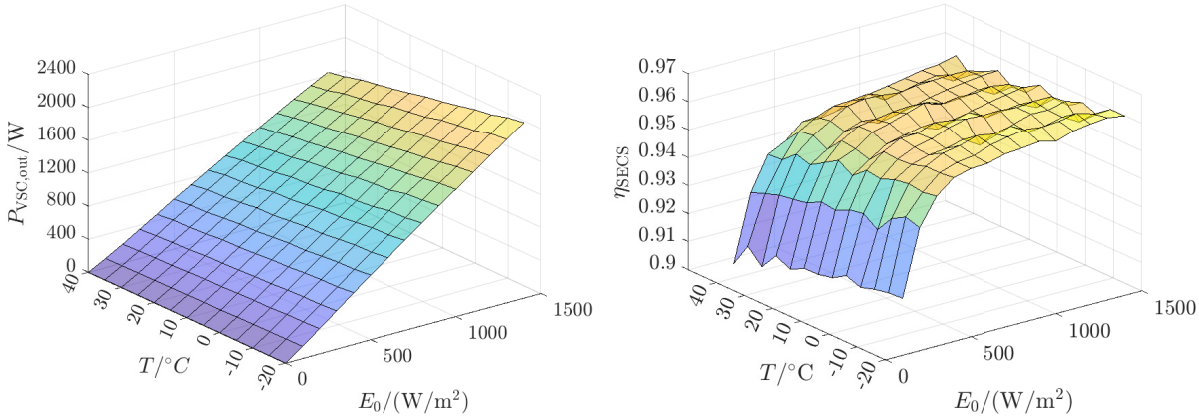

Fig. 6: SECS characteristic- and efficiency diagramm.

Entire system model

The entire system model contains the LUT based SECS, WECS and BESS, shown in Fig. 7. The EMS is realized with SIMULINK-Stateflow and designed for a high grade of energy self consumption of the head-end station. For this the sign of the power difference P_{Diff} is considered. With a positive sign the battery charges until SOC reaches the upper limit SOC_{max}. From then on power is fed into the grid. When P_{Diff} changes the sign the battery discharges. If SOC reaches a threshold at 50 % the uncritical load gets disconnected. When reaching the lower limit SOC_{min} the BESS is turned off and the power is supplied by the grid. If the BESS maximum charging resp. discharging power is exceeded the energy is fed into or supplied by the grid. A conversion of the global irradiance E_0 to South- and East-West alignments of the photoltaic modules is included. The time resolution of the measured data is 10 minutes. The timestamp allows the calculation of the sun position, as described in [10]. The measured wind speed at sensor height $v_{\mathrm{w,h_{ws}}}$ is converted to the wind speed at hub height $v_{\mathrm{w,h_{hub}}}$ (13) including the wind turbine radius r and roughness length z_0, given in Table II, Table IV and [11]. In addition to the energetic simulation with the measured data from Hilmersdorf further simulations with full-year datasets of the same time resolution for additional locations [12] are executed, see Table V. Using the MATLAB Parallel Computing Toolbox all combinations of the input configuration parameters, given by Table IV, are simulated. Every simulation iteration results the cumulated energies, calculated with (14). Furthermore the degree of self sufficiency α (15) and self consuption ε (16) are defined as follows.

$$v_{\mathrm{w,h_{hub}}} = v_{\mathrm{w,h_{ws}}} \frac{\ln\left(\frac{h_{\mathrm{hub}}-2r}{z_0}\right)}{\ln\left(\frac{h_{\mathrm{ws}}-2r}{z_0}\right)} \tag{13}$$

$$E = \int P \,\mathrm{d}t \tag{14}$$

$$\alpha = \frac{E_{\mathrm{SECS}} + E_{\mathrm{WECS}} - E_{\mathrm{feed-in}} - E_{\mathrm{charge}} + E_{\mathrm{discharge}}}{E_{\mathrm{SECS}} + E_{\mathrm{WECS}} - E_{\mathrm{feed-in}} - E_{\mathrm{charge}} + E_{\mathrm{discharge}} + E_{\mathrm{demand}}} \tag{15}$$

$$\varepsilon = \frac{E_{\mathrm{SECS}} + E_{\mathrm{WECS}} - E_{\mathrm{feed-in}}}{E_{\mathrm{SECS}} + E_{\mathrm{WECS}}} \tag{16}$$

Simulation results

One simulation of a detailed system with test input vectors takes about one hour to generate its own characteristic diagram. However the LUT based entire system model needs about 15 minutes for simulating 648 system configurations, given in Table IV. The measured energy demand of the head-end station is about $E_{\mathrm{Load}} = 16.5\,\mathrm{MWh}$ per year. Using the example of a single configuration Table VI shows the annual self sufficiency of the four different locations.

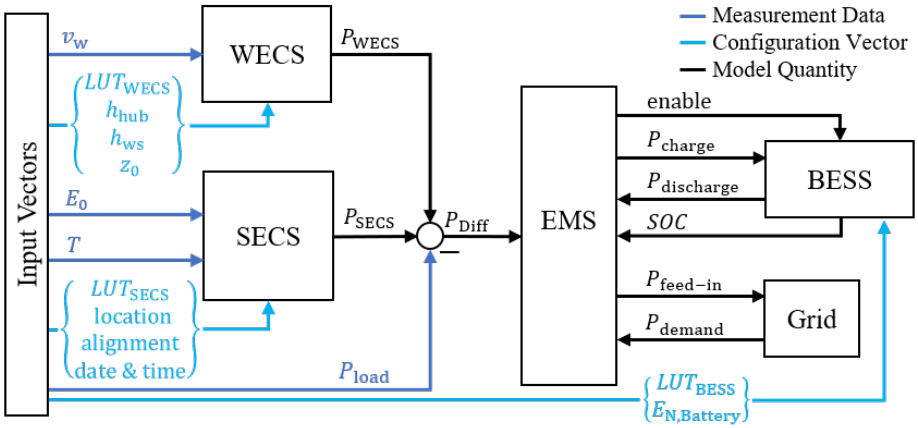

Fig. 7: Structure of entire renewable energy system model.

Table IV: Parameter space for simulating the entire system model.

Parameter	Quantity	Symbol	Parameter space
Location	4	-	{Fichtelberg; Görlitz; Hilmersdorf; Leipzig}
WECS Nominal power	3	$P_{WECS,N}$	$\{2.5; 5; 7.5\}$ kW
Hub height	3	h_{hub}	$\{10; 15; 20\}$ m
Number of PV modules	3	n_{PV}	$\{8; 16; 24\}$
Nominal battery capacity	3	$E_{b,N}$	$\{18.8; 37.6; 56.4\}$ kWh with $V_{b,N} = 360$ V
Alignment of PV Modules	2	α	$\{180°$ South; $90°$ East, $270°$ West$\}$
$\Rightarrow$ 648 Simulations			

Table V: Location with associated lat. φ, long. λ, metres above mean sea level (MAMSL), height of wind sensor h_{ws} and roughness length z_0.

Location	Characteristic	MAMSL	φ / °	λ / °	h_{ws} / m	z_0 / m
Fichtelberg	mountain top	1213	50.4283	12.9536	29	0.2
Görlitz	lowland, near city	239	51.1621	14.9506	12	0.03
Hilmersdorf	highland, industrial park	604	50.6761	13.1175	10	0.3
Leipzig	lowland, near airport	131	51.4347	12.2396	10	0.02

The maximum self sufficiency is reached at the Hilmersdorf and Fichtelberg site. For the mentioned configurations the monthly normalized energies on the energy demand for the SECS and WECS at the four locations are shown in Fig. 8. It can be seen that for this configuration the monthly WECS and SECS energies are fairly evenly distributed at the Hilmersdorf site, so this system configuration can supply a base load over the year. Furthermore a higher number of PV modules at the Görlitz and Leipzig site are neccesary to increase the energy availability during the summer months. Fig. 9 shows the self sufficiency for variable SECS, WECS and BESS configurations with a defined hub height and alignment of the PV modules. With an increasing system size the self sufficiency increases significantly.
This simulation tool requires a one year load, irradiance, temperature and wind speed profile at a specified location. In the first step these data are prepared with regard to uniform time resolution and time stamp. In addition the parameters of the prefered PV module type, wind turbine and battery are important for parameterization of the detailed system models. With predefined input vector combinations the characteristic diagrams of each detailed system are calculated. In the next step all combinations of the system configuration vectors consisting of the characteristic diagrams and parameter space, defined in e. g. Table IV, are simulated with the entire system model. The simulation results are a data basis for system optimization.

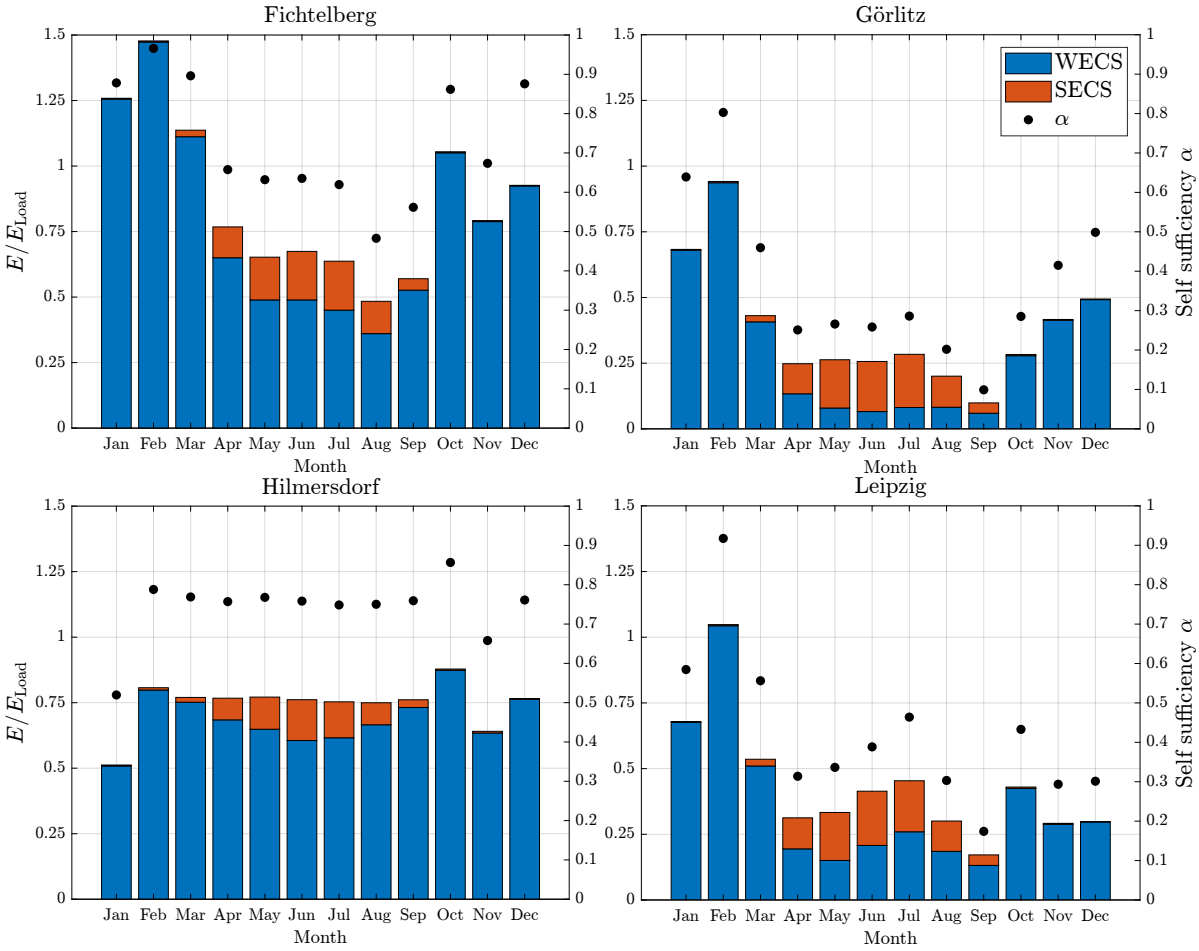

Fig. 8: Monthly normalized energies for SECS & WECS, system configuration mentioned in Table VI.

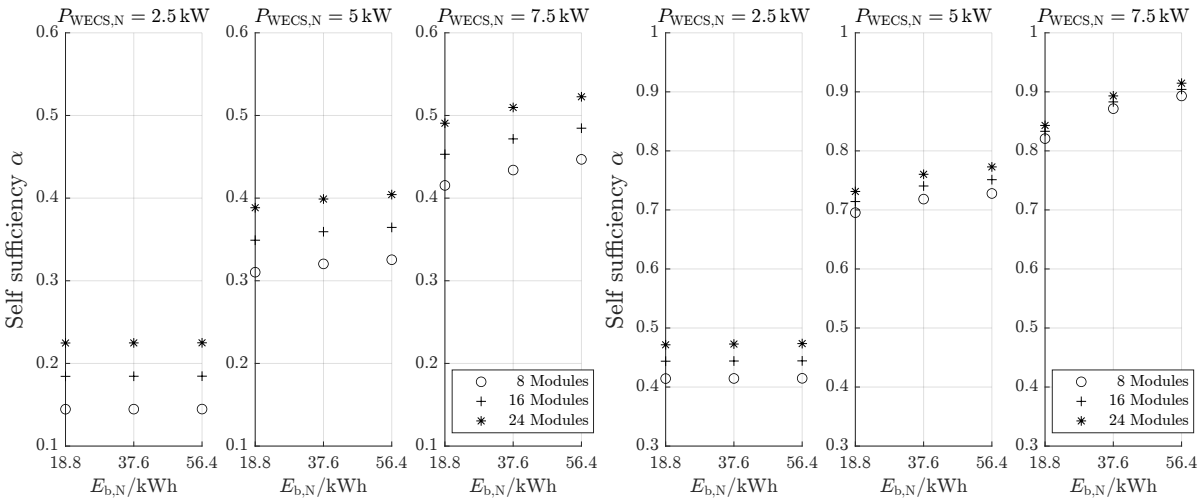

(a) Görlitz (b) Hilmersdorf

Fig. 9: Self sufficiency for variation of SECS, WECS and BESS configuration for $h_{\text{hub}} = 15\,\text{m}$ and $\alpha = 180°$ South.

Table VI: Location dependent annual self sufficiency for a single system configuration.

Configuration	$P_{\mathrm{WECS,N}} = 5\,\mathrm{kW}$	$h_{\mathrm{hub}} = 15\,\mathrm{m}$	$E_{\mathrm{b,N}} = 37.6\,\mathrm{kWh}$	$n_{\mathrm{PV}} = 16$	$\alpha = 180^{\circ}$ South
Location	Fichtelberg	Görlitz	Hilmersdorf	Leipzig	
Self sufficiency α	0.73	0.36	0.74	0.41	

Conclusion

This paper presents an energetic simulation with an entire system model of a hybrid renewable energy system consisting of a solar energy conversion system (SECS), wind energy conversion system (WECS) and a battery energy storage system (BESS) combined with an energy management system.
For reducing the simulation effort, in the first step, the detailed subsystem models, SECS, WECS and BESS are modeled separately in MATLAB/SIMULINK considering system losses e. g. power converter losses or joule losses of connections. Subsequent each subsystem is simulated with test input vectors to obtain a subsystem model with reduced complexity based on characteristic diagrams. In the second step these lookup table based models are brought together in combination with an energy management system to an entire system model. Thus, the entire system model allows an energetic simulation with full year periods of irradiance, temperature, wind speed and energy demand with regard to variable system configurations. Furthermore the entire system model can be used to optimize the detailed system specification regarding to site conditions and energy management requirements. Based on these calculations, a system design is currently already being developed and will be realized in 2022.

References

[1] Fischhaber S., Regett A., Schuster S. F., Hesse H.: Begleit- und Wirkungsforschung Schaufenster Elektromobilität (BuW): Ergebnispapier Nr. 18, Second- Life-Konzepte für Lithium-Ionen-Batterien aus Elektrofahrzeugen, 2016

[2] Stopka, U. et al.: Breitbandstudie Sachsen 2030. Studie im Auftrag des SMWA, TU Dresden, 2013

[3] Giroux P.: Loss Calculation in a BuckConverter Using SimPowerSystems and Simscape, https://www.mathworks.com/matlabcentral/fileexchange/35980-loss-calculation-in-a-buck-converter-using-simpowersystems-and-simscape, MATLAB Central File Exchange, Retrieved March 23, 2022

[4] Winkelnkemper M.: Reduzierung von Zwischenkreiskapazitäten in Frequenzumrichtern für Niederspannungsantriebe, TU Berlin, 2005

[5] Nguyen B. N., Nguyen V. T., Duong M. Q. , Le K. H., Nguyen H. H., Doan A. T.: Propose a MPPT Algorithm Based on Thevenin Equivalent Circuit for Improving Photovoltaic System Operation. Front. Energy Res., 18 February 2020

[6] Singh S., Manna S., Mansoori M. I. H., Akella A.K.: Implementation of Perturb & Observe MPPT Technique using Boost converter in PV System, CISPSSE-2020 India

[7] Hasaneen B. M., Mohammed A.: Design and Simulation of DC/DC Boost Converter, 12th International Middle-East Power System Conference, 2008, pp. 335-340

[8] Zammit D., Staines C. S., A Micallef A., Apap M.: Optimal Power Control for a PMSG Small Wind Turbine in a Grid- Connected DC Microgrid, CoDIT'18, Greece, 2018

[9] BMW Group, PressClub Global, https://www.press.bmwgroup.com/deutschland/article/attachment/T0189822DE/276981, Retrieved March 30, 2022

[10] Quaschning V.: Understanding Renewable Energy Systems, 2nd ed., London, 2016

[11] Namyslo J., Koßmann M.: Bestimmung effektiver Rauigkeitslängen an Windmessstationen aus topographischen Karten (TK-Verfahren), Deutscher Wetterdienst, www.dwd.de/DE/leistungen/gutachtenqpr/z0_aus_topo_karten.html, Retrieved March 23, 2022

[12] Deutscher Wetterdienst, Open Data Server: opendata.dwd.de, Retrieved March 23, 2022